

Design and analysis of in-plane and out-of-plane heterostructures based on monolayer tri-G with enhanced photocatalytic property for water splitting

Huijuan Wang^a, Xiaole Zheng^a, Xinxin Li^a, Linxin He^a, Jiasen Guo^a, Ying Chen^a, Hua Lin^a,
Jianfeng Tang^a, Chunmei Li^{a,*}

^a School of Materials and Energy, Southwest University, Chongqing 400715, China.

E-mail: lcm1998@swu.edu.cn

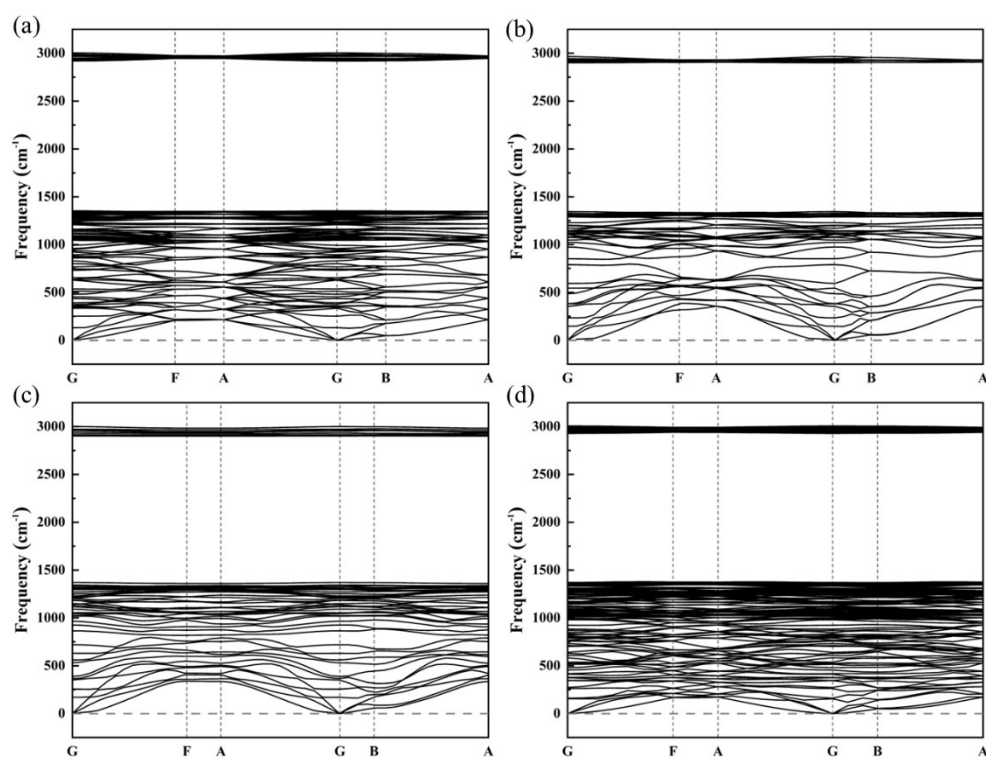


Fig. S1 Calculated phonon dispersions of four graphene conformers, (a) tri-G-A, (b) tri-G-B, (c) tri-G-C and (d) tri-G-D.

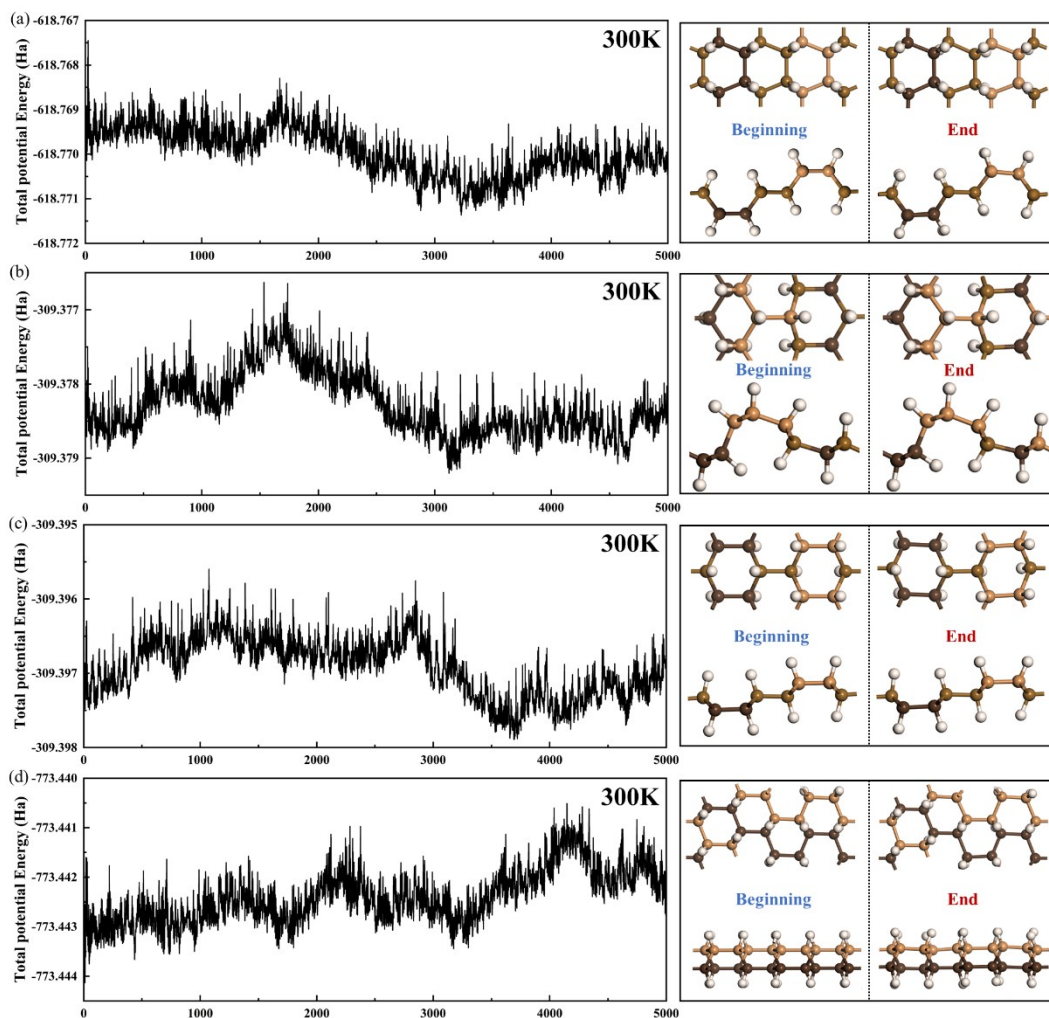


Fig. S2 The time-dependent potential energy fluctuation in (a) tri-G-A, (b) tri-G-B, (c) tri-G-C and (d) tri-G-D.

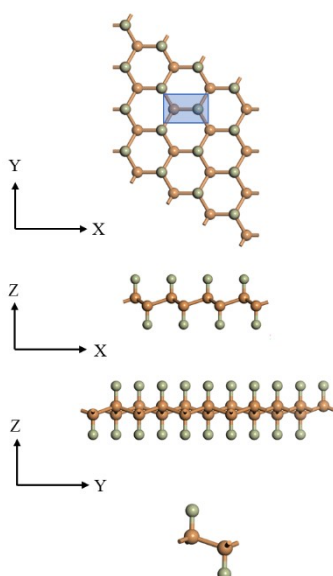


Fig. S3 Graphic structures of cha-G. Top view, side views, and the repetitive unit. Brown spheres indicate the C atoms while green spheres indicate H atoms.

S1 Absorption coefficient $I(\omega)$

The absorption coefficient $I(\omega)$ can be derived from the real part $\varepsilon_1(\omega)$ and the imaginary part $\varepsilon_2(\omega)$ of the dielectric function, which is given by

$$I(\omega) = \left[\sqrt{2\omega(\sqrt{\varepsilon_1(\omega)^2 - \varepsilon_2(\omega)^2} - \varepsilon_1(\omega))} \right]^{\frac{1}{2}}$$

In addition to above formula, the absorption coefficient can also be calculated by $\alpha(\omega) = k(2\omega/c)$, where k is the extinction coefficient.

Table S1 The bond populations of tri-G-A, tri-G-B, tri-G-C and tri-G-D.

	tri-G-A	tri-G-B	tri-G-C	tri-G-D
C-H	0.91	0.84	0.81	0.92
C-C	0.82	0.83	0.63	0.74

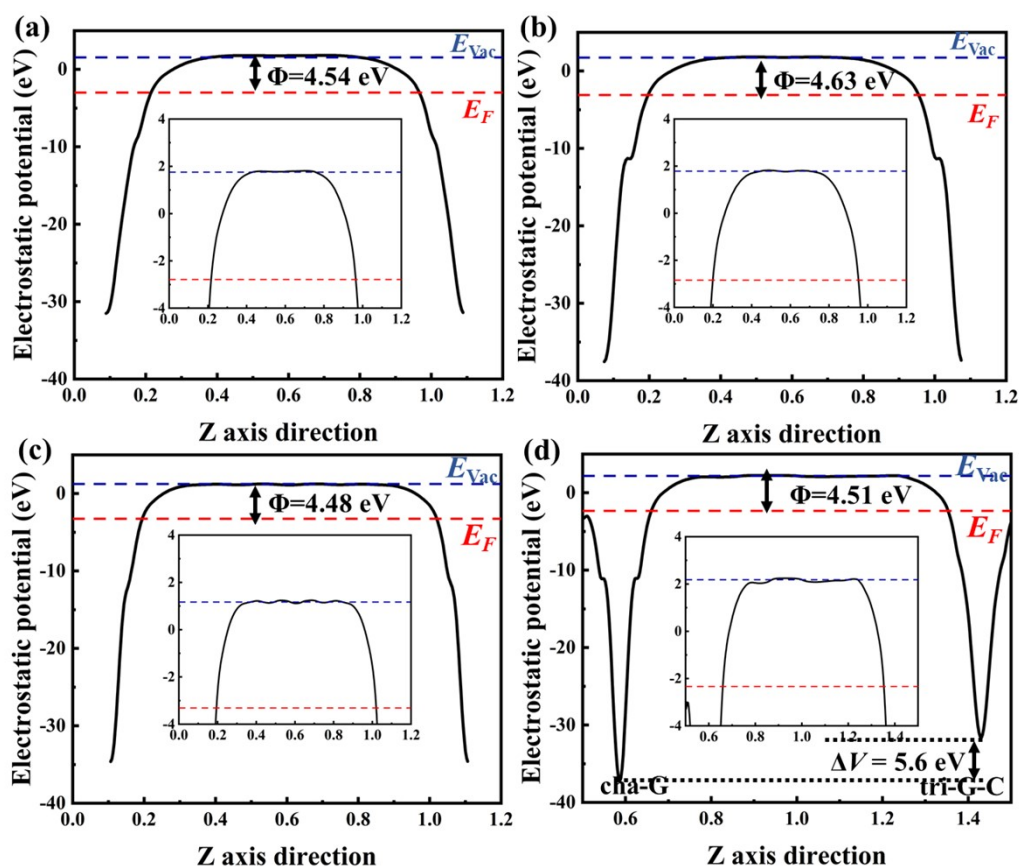
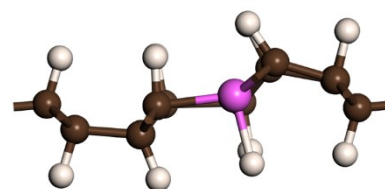
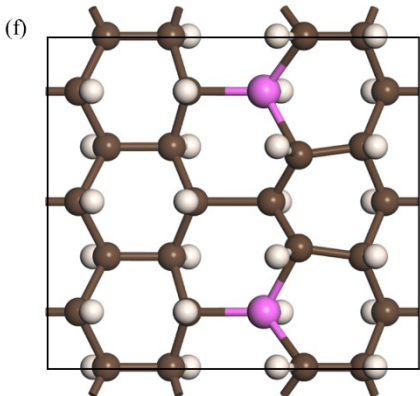
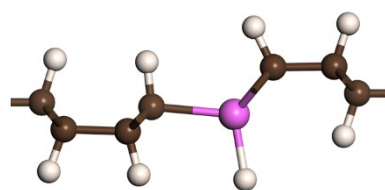
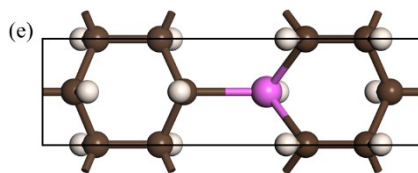
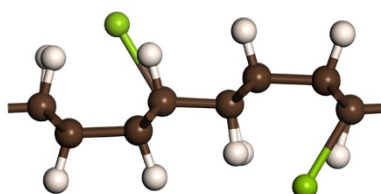
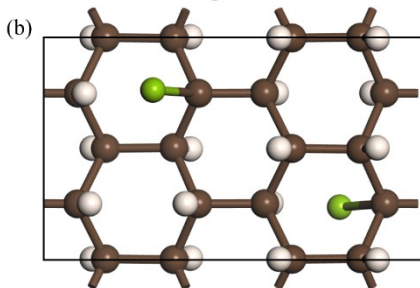
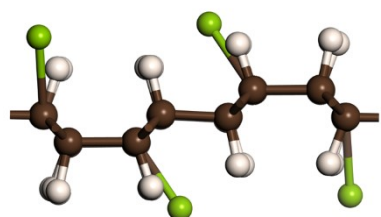
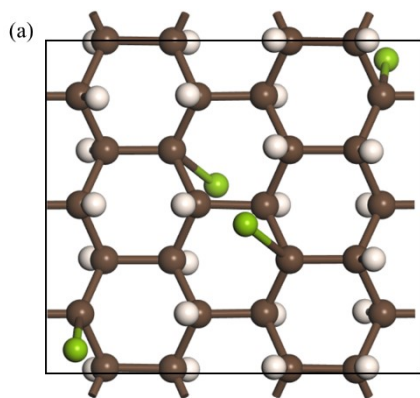
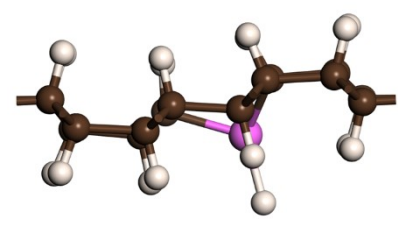
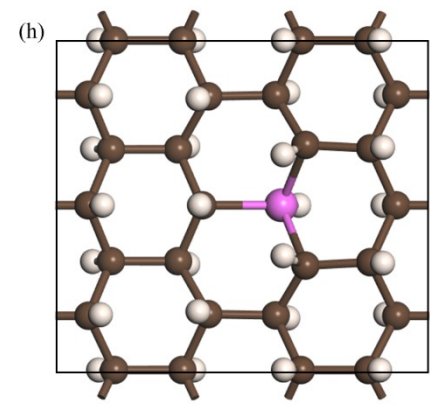
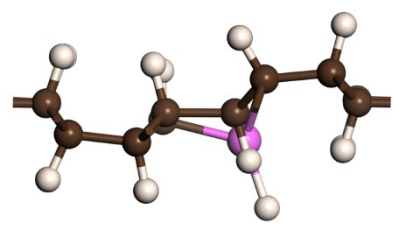
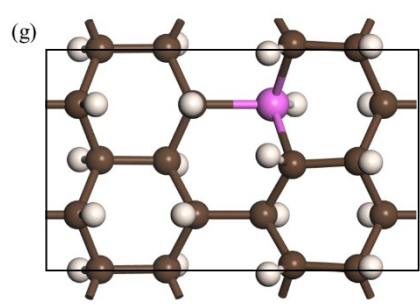
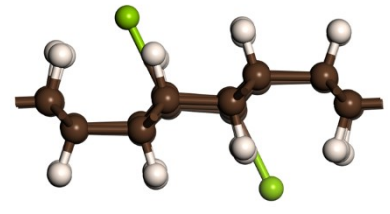
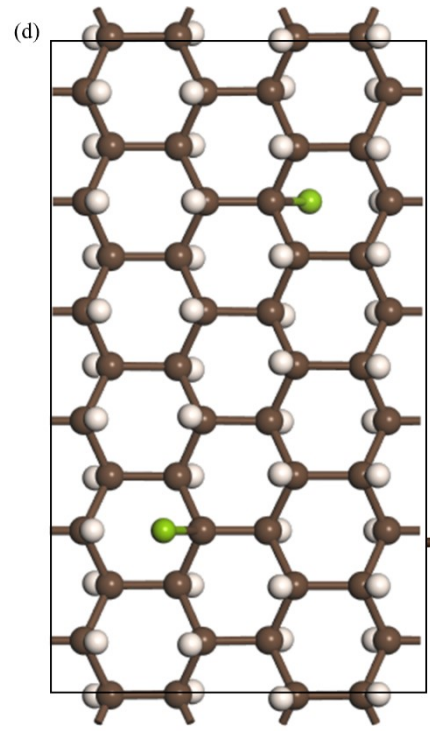
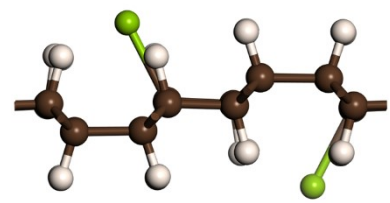
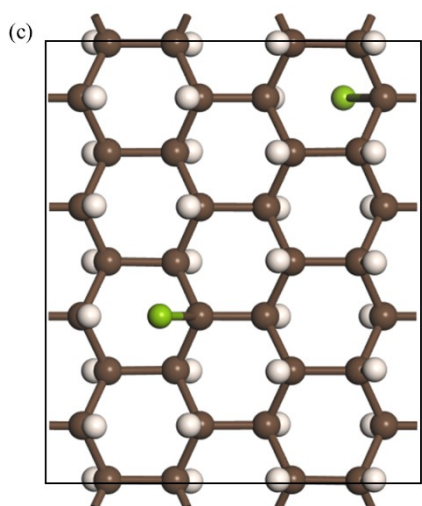


Fig. S4 (a-d) The estimated work functions of the individual tri-G-C, cha-G monolayers and tri-G-C/cha-G in-plane and out-of-plane heterostructures, respectively.





● H ● Li ● C ● Al

Fig. S5 The top and side views of optimized structures. Li-doped tri-G-C with the doping concentrations (atomic ratios) of (a) 8.33%, (b) 6.25%, (c) 3.13% and (d) 2.08%; Al-doped tri-G-C with the doping concentrations of (e) 6.25%, (f) 4.17%, (g) 3.13% and (h) 2.08%.

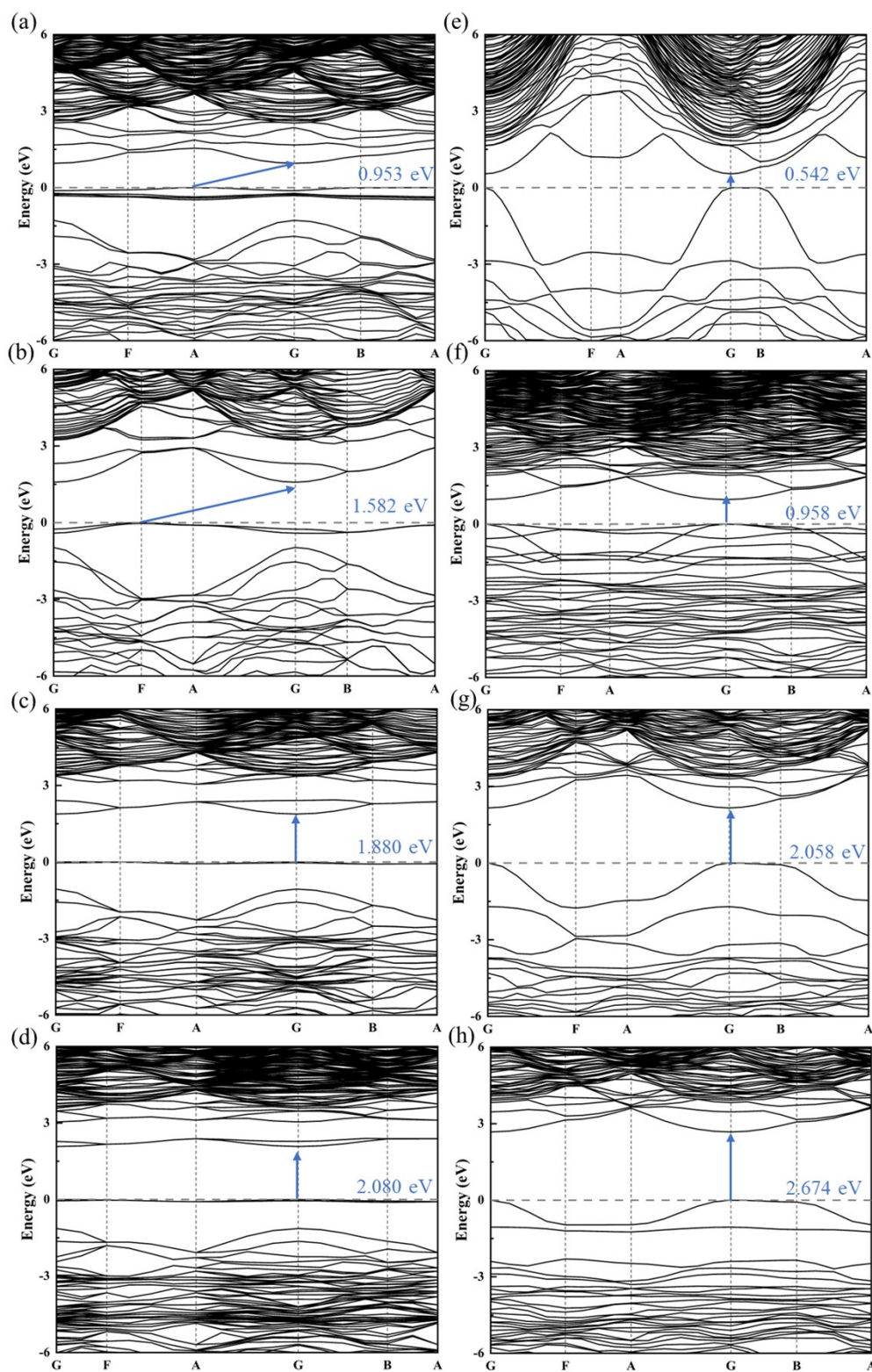


Fig. S6 Band structures of optimized models in HSE06. Li-doped tri-G-C with the doping concentrations (atomic ratios) of (a) 8.33%, (b) 6.25%, (c) 3.13% and (d) 2.08%; Al-doped tri-G-C with the doping concentrations of (e) 6.25%, (f) 4.17%, (g) 3.13% and (h) 2.08%.

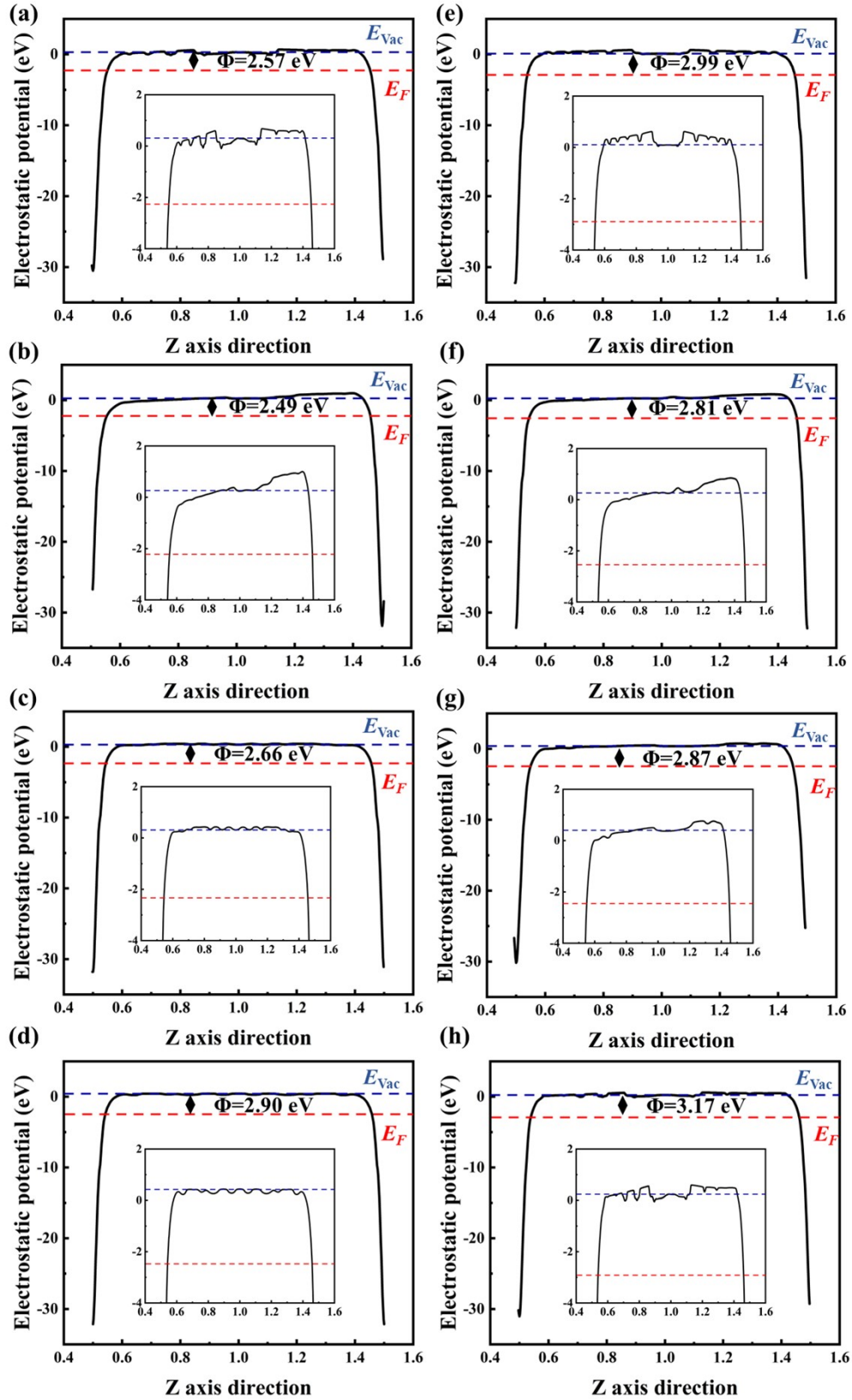


Fig. S7 The estimated work functions of Li-doped and Al-doped tri-G-C. Li-doped tri-G-C with the doping concentrations (atomic ratios) of (a) 8.33%, (b) 6.25%, (c) 3.13% and (d) 2.08%; Al-doped tri-G-C with the doping concentrations of (e) 6.25%, (f) 4.17%, (g) 3.13% and (h) 2.08%.

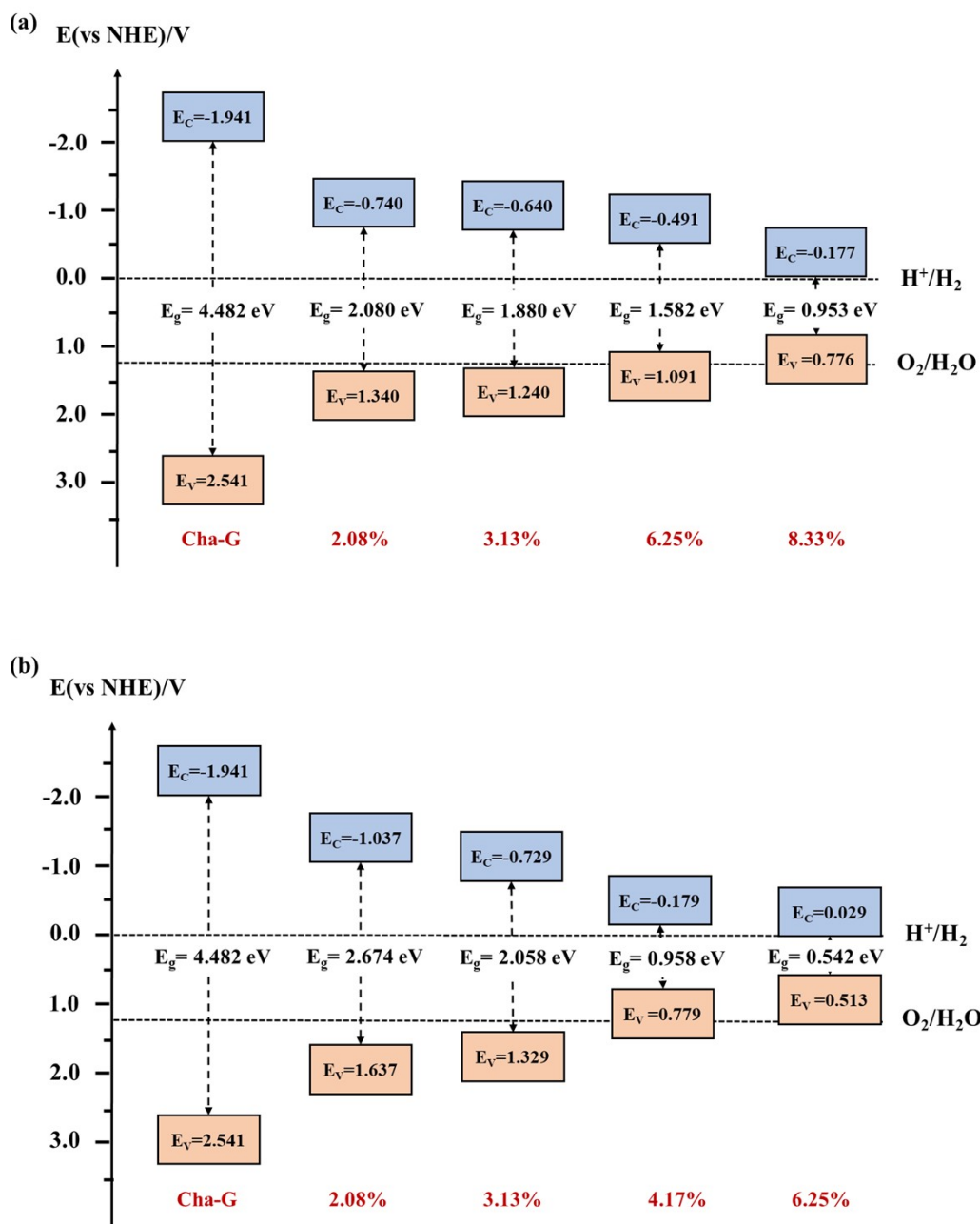


Fig. S8 (a) Band-edge positions of cha-G and Li-doped tri-G-C with the doping concentrations (atomic ratios) of 2.08%, 3.13%, 6.25% and 8.33%; (b) Band-edge positions of cha-G and Al-doped tri-G-C with the doping concentrations of 2.08%, 3.13%, 4.17% and 6.25%.

Table S2 Effective masses of electrons and holes in different doped tri-G-C.

		m_e^*/m_0	m_h^*/m_0	$D = m_h^*/m_e^*$	$D = m_e^*/m_h^*$
Li-doped	8.33%	1.313	3.708	2.824	0.354
	6.25%	1.108	3.433	3.098	0.323
	3.13%	1.156	3.906	3.378	0.296
	2.08%	1.347	3.748	2.783	0.359
Al-doped	6.25%	0.635	6.163	9.702	0.103
	4.17%	1.181	2.576	2.182	0.458
	3.13%	1.284	4.852	3.779	0.265
	2.08%	1.173	4.385	3.739	0.267